

# Spectral Geometric Verification: Re-Ranking Point Cloud Retrieval for Metric Localization

Kavisha Vidanapathirana<sup>1,2</sup>, Peyman Moghadam<sup>1,2</sup>, Sridha Sridharan<sup>2</sup>, Clinton Fookes<sup>2</sup>

**Abstract**—Although re-ranking methods are widely used in many retrieval tasks to improve performance, they haven't been studied in the context of point cloud retrieval for metric localization. In this letter, we introduce Spectral Geometric Verification (SpectralGV), for the re-ranking of retrieved point clouds. We demonstrate how the optimal inter-cluster score of the correspondence compatibility graph of two point clouds can be used as a robust fitness score representing their geometric compatibility, hence allowing geometric verification without registration. Compared to the baseline geometric verification based re-ranking methods which first register all retrieved point clouds with the query and then sort retrievals based on the inlier-ratio after registration, our method is considerably more efficient and provides a deterministic re-ranking solution while remaining robust to outliers. We demonstrate how our method boosts the performance of several correspondence-based architectures across 5 different large-scale point cloud datasets. We also achieve state-of-the-art results for both place recognition and metric-localization on these datasets. To the best of our knowledge, this letter is also the first to explore re-ranking in the point cloud retrieval domain for the task of metric localization. The open-source implementation will be made available at: <https://github.com/csiro-robotics/SpectralGV>.

## I. INTRODUCTION

Accurate 6 Degrees of Freedom (DoF) metric localization is an essential component in many applications ranging from mobile robotics to augmented reality. The task of accurate and robust re-localization in large-scale environments remains an open problem, and incorrect localization estimates can have dire consequences in safety-critical scenarios. When scaling this problem to city-scale environments (or larger), this task is made efficient through a hierarchical formulation which consists of two stages. This includes the place recognition step, which estimates a coarse place candidate, and a pose estimation step which estimates the alignment between the query and the top place candidate to obtain the 6DoF pose.

In the point cloud domain, the tasks of large-scale place recognition and 6DoF alignment (*i.e.*, registration) have been explored largely in isolation [1]–[3]. Recently, several methods have combined the two tasks to offer a complete solution for large-scale metric localization [4]–[6]. They follow a correspondence-based approach, where local-features are used to estimate correspondences between the query point cloud and the top-candidate returned by global-descriptor matching, and the transformation is obtained using

the estimated correspondences. Although not yet explored in the point cloud domain, re-ranking of the top retrieved candidates can be used to improve retrieval performance. Re-ranking has been well studied in other domains of information retrieval [7], [8] but it has not received much attention in the task of point cloud retrieval. While the same re-ranking methods used in other domains can be adopted to point clouds, these methods are not suited to fully exploit the precise 3D geometry information present in point clouds.

In this paper, we introduce a spectral geometric verification based re-ranking approach which performs re-ranking by estimating a spatial consistency score between the query and each retrieved candidate. Baseline geometric verification methods require registering the query point cloud with each candidate to calculate the registered-inlier-ratio to be used as a fitness score for re-ranking. Our method does not require registration and is therefore more efficient, while also being deterministic and robust to outlier correspondences. Using the correspondence compatibility graph introduced in Spectral Matching [9], we demonstrate how the optimal inter-cluster score of the adjacency matrix of this graph represents a spectral confidence score on the geometric compatibility of two point clouds, hence allowing it to be used as a fitness score for re-ranking. Our re-ranking formulation allows direct integration with any architecture that extracts both local and global features for a given point cloud, without modifying the architectures and without further training of learning-based methods.

Our main contributions are summarized as follows:

- We introduce a spectral geometric verification based method for re-ranking point cloud retrieval which does not require registration of the query with each retrieved candidate.
- Our method can be readily integrated with existing metric localization methods without any modification to their architectures and without further training. It is an architecture agnostic method and shows no bias towards datasets allowing it to generalize well.
- We integrate our method with state-of-the-art architectures and demonstrate performance improvements across 5 large-scale datasets in all evaluation settings.
- We study the suitability of multiple types of re-ranking methods for point cloud retrieval. We empirically demonstrate how all geometric verification based re-ranking methods are robust, while ours is the most efficient as it can be parallelized to re-rank all top-k candidates simultaneously.

<sup>1</sup> Robotics and Autonomous Systems Group, DATA61, CSIRO, Australia. E-mails: *firstname.lastname@data61.csiro.au*

<sup>2</sup> School of Electrical Engineering and Robotics, Queensland University of Technology (QUT), Brisbane, Australia. E-mails: {*s.sridharan, c.fookes*}@qut.edu.au

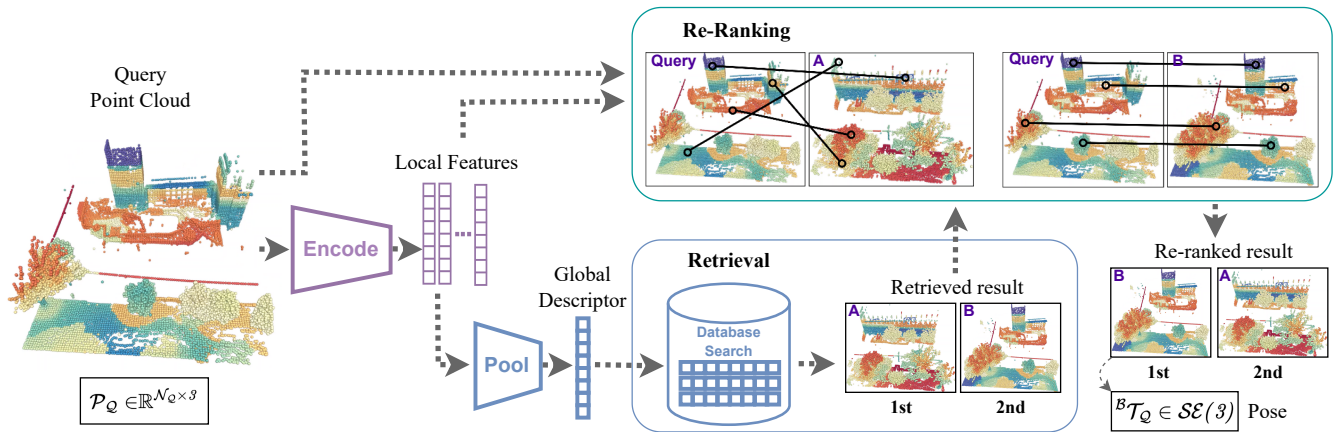


Fig. 1: Overview of our SpectralGV method. Local features are extracted from the query point cloud using an encoder and then aggregated to form a global descriptor which is used in the ‘Retrieval’ block to find the top-k place candidates ( $k=2$  in the diagram). The local features and point cloud are used for re-ranking the retrieved candidates in the ‘Re-Ranking’ module which estimates a matching confidence based on the spatial consistency of point correspondences (black lines). In this example, retrieved point cloud ‘B’ better satisfies the geometric constraints and is therefore ranked higher than ‘A’ after re-ranking. The 6DoF pose estimate  $\mathcal{T}_Q$  is obtained using the top re-ranked candidate. Point clouds are coloured based on the t-SNE embeddings of local features to better visualize the point correspondences.

## II. RELATED WORK

### A. Place Recognition

Large-scale place recognition is formulated as a retrieval problem where methods encode each point cloud to a compact vector representation that can be used for querying a database of previously visited places. Global descriptors can be categorised as handcrafted [10], [11], hybrid [12], and end-to-end [13]–[17]. While handcrafted method such as ScanContext [10] and hybrid methods such as Locus [12] still act as strong baselines, end-to-end methods have demonstrated superior performance [15], [18].

End-to-end methods define a neural network that maps point clouds into a compact global descriptor. PointNetVLAD [13] first introduced an end-to-end trainable global descriptor by extracting local features using PointNet [19] and aggregating them using NetVLAD [20]. Several works such as LPD-Net [14] and MinkLoc3D [15] have been proposed to address the limitations of PointNetVLAD. Recently, LoGG3D-Net [18] demonstrated how using joint constraints on the local and global embeddings during the training can lead to improved performance. In this paper, we demonstrate that the performance of these successful methods can be further improved by a large margin via our proposed re-ranking solution.

### B. Metric localization

DH3D [4] pioneered correspondence-based metric localization using LiDAR data by proposing the unification of global place recognition with local 6DoF refinement. They used a simultaneous detect-and-describe formulation to extract local features, NetVLAD to generate a global descriptor, and RANSAC [21] to estimate the 6DoF pose. LCDNet [5] proposed the use of a differentiable relative pose head based

on Unbalanced Optimal Transport (UOT) [22] to match local features. EgoNN [6] extended the MinkLoc3D architecture for the task of metric localization with the addition of keypoint detection and saliency prediction modules. Global descriptors formed by GeM [7] pooling were used for retrieval and RANSAC was used for pose estimation.

The re-ranking method proposed in this paper can be readily integrated into all the above correspondence based metric localization methods [4]–[6] as well as place recognition methods such as [18] which produce discriminative local features. This integration can be performed without any modification to the respective network architectures.

### C. Re-ranking

In many retrieval problems, re-ranking methods take the initial retrieved candidates and re-order them such that correct candidates will be ranked higher. These methods can be categorised as those which use only the global descriptors and those which use both global and local features. Re-ranking methods which use only global descriptors can be classified under Query Expansion (QE) [7] methods that use first-order neighbour information and methods that use higher-order neighbour information such as k-reciprocal [23], [24] and region-diffusion [25]. QE methods take the nearest neighbours of the query and generate an updated query which is used to retrieve a new set of candidates. The updated query is an aggregation of the initial top-candidates (e.g., average-QE, alpha-QE [7]). Higher-order methods consider the neighbours-of-neighbours of the query and are non-trivial to extend to large-scale scenarios [8].

As opposed to general information retrieval tasks (e.g., text-retrieval), when re-ranking in the context of localization (using either images or point clouds), the geometric cues present in the scene can be used to aid the re-ranking. For

this, the local features can be used in addition to the global descriptors to verify geometric consistency between the query and the retrieved candidates. This family of geometric-verification based re-ranking has become popular for visual place recognition [26]–[28]. DELG [26] used RANSAC [21] based geometric verification on the local features for re-ranking. PatchNetVLAD [27] compared RANSAC based re-ranking with a novel rapid-spatial-scoring mechanism for efficient geometric verification on images. RRT [8] explored learning-based image re-ranking using transformers.

### III. PROPOSED METHOD

In this section, we discuss each component in our proposed re-ranking based metric localization approach. The overall pipeline is depicted in Fig. 1.

#### A. Problem Formulation

Our approach to metric localization is split into 3 sub-tasks: retrieval, re-ranking and 6DoF pose estimation.

**Retrieval:** The initial sub-task of point cloud retrieval is formulated as follows. Given a point cloud  $\mathcal{P} \in \mathbb{R}^{N \times 3}$  representing varying number of  $N$  points with associated 3D position, a mapping function  $\Phi$  such that

$$\Phi : \mathcal{P} \rightarrow (\mathcal{F}, g) \quad (1)$$

is learnt that represents the point cloud  $\mathcal{P}$  as a set of local features  $\mathcal{F} \in \mathbb{R}^{N \times d'}$ , and also as a fixed-size vector global descriptor  $g \in \mathbb{R}^d$ . During retrieval, the global descriptor  ${}^Qg$  of the query point cloud  ${}^Q\mathcal{P}$  is matched with a database of global descriptors of previously visited places to obtain the top-k retrieval candidates,

$${}^Q\mathcal{L}_R = \{{}^Q\mathcal{P}_{R_1}, \dots, {}^Q\mathcal{P}_{R_k}\}, \quad (2)$$

where  ${}^Q\mathcal{L}_R$  is ordered based on similarity of retrieved global descriptors with  ${}^Qg$ . For methods that do not use re-ranking,  ${}^Q\mathcal{P}_{R_1}$  is taken as the solution for place recognition.

**Re-Ranking:** In the second sub-task, geometric verification based re-ranking techniques aim to calculate a geometric ‘fitness score’ between the query and each retrieved candidate:  ${}^QS = \{s_1, \dots, s_k\}$ , where the ‘fitness score’ measures the respective geometric consistency between the query and each retrieved candidate using point correspondences estimated by matching the local features  $\mathcal{F}$ .

The top-k candidates are then re-ranked by sorting based on  ${}^QS$  to obtain,

$${}^Q\mathcal{L}_{RR} = \{{}^Q\mathcal{P}_{RR_1}, \dots, {}^Q\mathcal{P}_{RR_k}\}, \quad (3)$$

where the list  ${}^Q\mathcal{L}_{RR}$  is a permutation/re-ordering of the list  ${}^Q\mathcal{L}_R$ . A successful re-ranking method will ensure that,

$$\mathcal{D}({}^Qx, {}^Qx_{RR_1}) \leq \mathcal{D}({}^Qx, {}^Qx_{R_1}), \quad (4)$$

for all queries  $Q$  where  ${}^Qx, {}^Qx_{R_1}, {}^Qx_{RR_1}$  are the ground-truth geo-locations of  ${}^Q\mathcal{P}, {}^Q\mathcal{P}_{R_1}, {}^Q\mathcal{P}_{RR_1}$  respectively, and  $\mathcal{D}$  represents Euclidean distance. The above inequality assumes that the correct retrieval is present in the initial list of retrieved candidates, and the equality arises when the top-1 result of the initial retrieved candidates is correct. We

note that re-ranking methods which are not robust will occasionally violate this inequality (due to failure cases such as noisy inputs, degenerate scenes). In some instances, they will reduce retrieval performance after re-ranking. We define ‘Robust’ re-ranking methods as those which always preserve this inequality. We empirically demonstrate how, for point cloud retrieval, all geometric-verification based re-ranking methods are robust, while ours is the most efficient as it does not require registration and can be parallelized to re-rank all retrieved candidates at once.

**Pose Estimation:** During the third sub-task, the pose estimation is obtained by registering the query  ${}^Q\mathcal{P}$  with the top-1 re-ranked candidate  ${}^Q\mathcal{P}_{RR_1}$  to obtain their relative transformation:  ${}^Q\mathcal{T}_{RR_1} \in SE(3)$ . This transformation can be estimated using any point cloud registration technique. Typically, for LiDAR-based metric-localization, since local features and global descriptors are extracted concurrently, correspondence-based registration techniques using robust estimators such as RANSAC are preferred over alternatives.

This paper focuses on the second sub-task of re-ranking, and the proposed method can be readily incorporated with existing architectures which support the formulation presented in Eq.1 to enable global descriptor based retrieval and local feature correspondence based registration. Baseline point cloud re-ranking can be performed using geometric verification of local feature correspondences using a robust estimator such as RANSAC [21]. This family of methods first register the query point cloud with each of the top-k retrieved point clouds, calculate the point inlier-ratio after registration, and then sort the retrievals based on the Registered-Inlier-Ratio (RIR). This type of re-ranking is inefficient as it requires registering the query with each retrieval. In this paper, we introduce a spectral fitness score as an alternative to the RIR for geometric verification based re-ranking.

#### B. Spectral Geometric Verification

Inspired by the Spectral Matching method introduced in [9], we define an un-directed graph  ${}^Q\mathcal{G}_R = (\mathcal{V}, \mathcal{E})$  between the query  ${}^Q\mathcal{P}$  and each retrieved candidate  ${}^Q\mathcal{P}_R \in {}^Q\mathcal{L}_R$ . Vertices  $\mathcal{V} = \{1, \dots, n\}$  represent the  $n$  elements in the set of local point correspondences  ${}^Q\mathcal{C}_R$  between the two point clouds obtained by nearest-neighbour search on their local features. Here  $c_i \in {}^Q\mathcal{C}_R$  is denoted as  $c_i = (x_i, y_i)$ , where  $x_i \in {}^Q\mathcal{P}, y_i \in {}^Q\mathcal{P}_R$  are the corresponding points from the two point clouds. The edges  $\mathcal{E} \subseteq \mathcal{V} \times \mathcal{V}$  represent the spatial compatibility score of these correspondences (defined later). The motivation here is that this graph will form clusters of nodes which have high spatial consistency with each other, and the largest cluster of this graph is statistically likely to be the inlier-correspondences, as it is highly unlikely that outlier correspondences will be spatially consistent with the inliers or with each other as shown in [9].

${}^QM_R$  is used to represent the adjacency matrix of this graph, and noted as  $M$  for brevity.  $M \in \mathbb{R}^{n \times n}$  is a symmetric matrix of all positive elements where each element  $m_{i,j}$  represents a spatial compatibility score between the correspondences  $c_i, c_j$ . Specifically,  $m_{i,j}$  measures how well

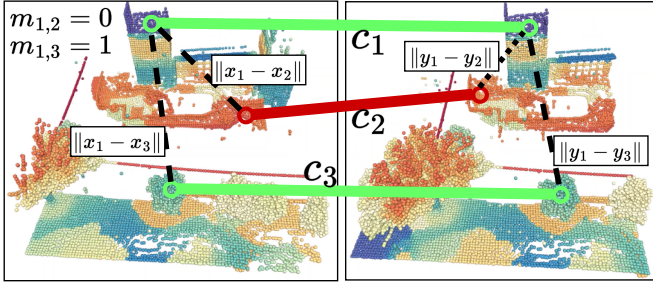


Fig. 2: Visualization of values in the adjacency matrix  $M$ . Out of the 3 depicted correspondences, the green ones ( $c_1, c_3$ ) are inliers and the red ( $c_2$ ) are outliers. Inlier correspondences will preserve their spatial consistency (low  $d_{1,3}$ ) and from strong edges in  $M$  (high  $m_{1,3}$ ), while the outliers will not form strong edges with the inliers (low  $m_{1,2}$ ).

the pairwise geometry of two points in the query point cloud are preserved after matching them with two points in the retrieved point cloud. This is defined as,

$$m_{i,j} = [1 - \frac{d_{ij}^2}{d_{thr}}]_+, d_{ij} = | \|x_i - x_j\| - \|y_i - y_j\| |, \quad (5)$$

where  $[\cdot]_+ = \max(\cdot, 0)$  ensures a non-negative value for  $m_{i,j}$ , and  $d_{thr}$  controls the sensitivity to the length difference. As depicted in Fig. 2, correspondence pairs with length difference larger than  $d_{thr}$  are considered incompatible and get a zero value in  $M$ , while pairs which preserve their length relationships obtain high positive scores.

The task of finding the inlier correspondences is formulated as finding the cluster  $\hat{C} \subseteq \mathcal{Q}\mathcal{C}_R$  of correspondences that maximize the inter-cluster spatial compatibility score,

$$s = \sum_{c_i, c_j \in \hat{C}} m_{i,j}, \quad (6)$$

subject to the constraint that no pairs of incompatible correspondences are present in  $\hat{C}$ . By representing the cluster  $\hat{C}$  using a binary indicator vector  $v$  such that  $v(c_i) = 1$  if  $c_i \in \hat{C}$  and zero otherwise, we can re-write the inter-cluster score in Eq.6 as  $s = v^T M v$ . Given this formulation the indicator vector that obtains the maximum inter-cluster score can be computed as,

$$v^* = \operatorname{argmax}(v^T M v). \quad (7)$$

As demonstrated in [9], the compatibility constraint and the integer constraint on  $v$  can be relaxed and it's norm can be fixed to 1 since only the relative values of it's elements are important. Then, Eq. 7 can be represented as,

$$v^* = \operatorname{argmax} \left( \frac{v^T M v}{v^T v} \right) \quad (8)$$

where  $v^*$  can be approximated using the principal eigenvector of  $M$  according to the Rayleigh quotient.

While the methods of Spectral Matching [9] and its recent variants [29] focus only on using  $v^*$  to solve the registration

problem, they do not make use of the maximized score:  $s^* = v^{*T} M v^*$ . In this paper we demonstrate how this maximized score can be interpreted as a score representing the geometric consistency between point clouds and therefore can be used as a fitness score for geometric verification based re-ranking.

Using this interpretation of  $s^*$ ,  $\mathcal{Q}\mathcal{L}_{RR}$  can be obtained by sorting  $\mathcal{Q}\mathcal{L}_R$  based on descending  $s^*$  calculated between the query  $\mathcal{Q}\mathcal{P}$  and each  $\mathcal{Q}\mathcal{P}_R \in \mathcal{Q}\mathcal{L}_R$ . This formulation re-ranks the initial retrievals based on the spatial consistency of local feature correspondences with the query. Thus it is a form of geometric verification. Additionally, as demonstrated in [9], this spectral score is statistically robust against outlier correspondences which results in a robust geometric verification method as substantiated by our results. Finally, this formulation does not need to solve the registration between the query and each candidate, making it far more efficient.

## IV. EXPERIMENTS

### A. Implementation

We integrate our Spectral Geometric Verification (SGV) re-ranking method with 2 metric localization architectures EgoNN [6], LCDNet [5] and one place recognition architecture LoGG3D-Net [18], which outputs discriminative local features in addition to the global descriptor. Our re-ranking method takes as input the points and local features of the query and candidate point clouds and outputs a fitness score for each candidate. We use the power-iteration method to efficiently approximate the leading eigenvector  $v^*$  in Eq. 8. The calculation of our spatial-consistency fitness score is parallelized to process all candidates simultaneously.

For EgoNN and LCDNet we use the detected keypoints and associated features. Since LoGG3D-Net does not perform keypoint detection, we can output local features from any point in the second half of its UNet architecture. We test 2 settings: LoGG3D-Net-dense which takes points from the final output of the local features (these points have the same resolution as the input point cloud), and LoGG3D-Net-sparse which takes points from the layer after 1 transposed convolution from the UNet bottleneck (these points have 1/8th the resolution of the original point cloud). For EgoNN we use the pre-trained model released by the authors which was trained in the same train set as used in this paper. LoGG3D-Net and LCD-Net are trained on a cluster of P100-16GB GPUs. For LCD-Net we use a batch size of 4 and train for 150 epochs using identical hyper-parameters from [5].

### B. Datasets

We evaluate on five public LiDAR datasets, all of which are collected from a mobile platform in multiple dynamic urban environments. We use identical training sets as used in [6] and train on portions of MulRan [30] and Apollo-SouthBay [31] datasets. For evaluation we define 2 settings (easy and hard) where the easy setting consists of the evaluation sequences proposed in [6] (MulRan Sejong [30], Apollo-SouthBay [31] and KITTI odometry [32] datasets), and for the hard setting we introduce additional sequences (unseen during training) in which current methods struggle

Train/Test Split	Length	Step	Number of scans
<i>Train split:</i>			
MulRan [30]: Sejong (0.1/02)	19 km	0.2 m	35,871
SouthBay [31]: excl. Sunnyvale	37 km	1.0 m	72,706
<i>Test split (Easy):</i>			
MulRan [30]: Sejong (01/02)	4 km	0.2 m	(database / query) 3,764 / 3,453
SouthBay [31]: Sunnyvale	38 km	1.0 m	48,959 / 16,999
KITTI [32]: Sequence 00	4 km	0.1 m	1,620 / 621
<i>Test split (Hard):</i>			
MulRan [30]: DCC (01/02)	4.9 km	10.0 m	469 / 307
ALITA [33] (R1 val:5)	1.4 km	3-20 m	107 / 84
KITTI-360 [34]: Sequence 09	10.5 km	3.0 m	766 / 398

TABLE I: Details of training and evaluation sets.

to generalize using MulRan DCC, KITTI-360 [32] and the ALITA [33] datasets. In MulRan DCC, sequences 01 and 02 are used as database and query sets. In KITTI-360, sequence 09 is used with the first 300 seconds of the sequence as a database and the rest as queries. In ALITA, we evaluate on the data released in round 1 of the UGV Challenge at ICRA 2022 and use the validation sequence 5. Details on the number of scans and sampling step lengths of the training and evaluation splits are given in Table. I.

### C. Evaluation Criteria

For the task of place recognition, we compute the similarity between the global descriptors of each query point cloud with global descriptors from the database set in each sequence and get the top k-retrieval candidates. The top-k retrieval candidates are then re-ranked using their local features to obtain the refined top-k retrievals. We report Recall@k (Rk) (for k = 1 and 5) metrics for 5 and 20 m thresholds. We also use the Mean Reciprocal Rank (MRR) as it serves as a scalar summary of the Recall@k curve. The Rk and MRR metrics are defined as

$$MRR = \frac{1}{|Q|} \sum_{q \in Q} \frac{1}{r_q}, \quad Rk = \frac{1}{|Q|} \sum_{q \in Q} \begin{cases} 1, & \text{if } r_q \leq k \\ 0, & \text{otherwise} \end{cases} \quad (9)$$

where  $r_q$  is the rank of the first true-positive retrieval for a given query  $q \in Q$ . We report both metrics as percentages.

In the task of metric localization, for queries which have top-1 retrievals within 20m, we calculate the 6DoF relative pose between the query and the retrieval and evaluate that in comparison to the ground truth transformation. Incorrect top-1 retrievals are excluded from localization evaluation. We use the 3 standard metrics: the Success rate is the percentage of pose estimates within 2m and  $5^\circ$  threshold from the ground truth, the Relative Rotation Error (RRE) and Relative Translation Error (RTE) metrics are as defined in [29].

### D. Results

1) *Place recognition evaluation:* We compare place recognition performance using the handcrafted method ScanContext [10], hybrid method Locus [12] and end-to-end learning methods MinkLoc3D [15], DiSCO [35], DH3D [4], EgoNN [6], LCDNet [5] and LoGG3D-Net [18]. Table II shows coarse-level place recognition results on the ‘easy’ evaluation sets while Table. III shows the corresponding

results in the ‘hard’ evaluation sequences. On the ‘easy’ evaluation set, we see that LoGG3D-Net outperforms the previous state-of-the-art EgoNN on average performance across all evaluation metrics. For the methods which also output local features (EgoNN, LCDNet and LoGG3D-Net), we also evaluate performance after re-ranking. The results on the ‘easy’ set are already saturated prior to re-ranking but we still see improvements (or on-par results) for all methods after re-ranking using SGV. LoGG3D-Net + SGV obtains the best performance overall on the ‘easy’ datasets.

On the ‘hard’ evaluation setting all methods do worse as not only are these sequences unseen during training, but they also contain difficult evaluation scenarios such as reverse/orthogonal revisits and lane offsets during revisits. Therefore, the performance gain after re-ranking is much more pronounced on the ‘hard’ evaluation set. We observe that LoGG3D-Net which fails to generalize to the ALITA dataset shows an improvement of 32.5 MRR after re-ranking which is more than double the initial MRR while also almost quadrupling R1 after re-ranking. The results after re-ranking using our SGV are better for all methods in all datasets. This demonstrates that our method improves retrieval performance on all datasets while being architecture agnostic.

2) *Re-ranking evaluation:* We explore different methods for re-ranking of point cloud retrievals. We evaluate on the ‘hard’ evaluation sequences using the 5 and 20m revisit thresholds using the Recall@1, MRR metrics and the time taken (in ms) for re-ranking. We present results under two settings: using 2 and 20 top-k candidates from the initial retrieval. The re-ranking methods are compared in Table. IV.

We group the re-ranking methods into 3 categories. The first category consists of methods which only use the global descriptor. For this we evaluate two Query Expansion (QE) methods: Average-QE and Alpha-QE [7]. We observe that Average-QE does not produce a performance improvement in any setting. In fact it reduces performance of the baseline when using 20 top-k candidates. This is because majority of the global descriptors in the initial retrieval are incorrect matches, hence averaging these in to the new query simply produces a noisy query. For Alpha-QE we see some improvements in Recall@1 when using only the top-2 candidates, and also notice degrading performance with increasing  $n_{topk}$ . As noted in other studies [8], it is not possible to tune the parameters of these methods such that they perform well on all datasets. While this family of methods are far more efficient in performing re-ranking, their results are not useful.

The second family consists of geometric verification (GV) methods that perform re-ranking based on the registered-inlier-ratio (RIR). For this we test 3 robust geometric estimators to perform the registration: RANSAC [21], FGR [36] and TEASER++ [37]. For RANSAC and FGR we use the efficient implementations provided in the Open3D [38] library. We observe that all RIR methods produce a significant improvement in performance in all settings. RANSAC obtains the best performance in the RIR family (group (b) in Tab. IV) while also being the most efficient.

The final family of re-ranking methods consists of geo-

	MulRan Sejong				Apollo-SouthBay				KITTI				Average			
	5 m		20 m		5 m		20 m		5 m		20 m		5 m		20 m	
	R1	R5	R1	R5	R1	R5	R1	R5	R1	R5	R1	R5	R1	R5	R1	R5
MinkLoc3D* [15]	82.3	94.4	92.1	96.6	77.2	93.8	95.0	98.3	95.7	96.9	97.7	98.0	85.0	95.0	94.9	97.6
DiSCO* [35]	94.0	97.5	95.8	98.1	95.1	96.6	95.4	97.0	90.7	91.3	92.3	94.5	93.2	95.1	94.5	96.5
DH3D* [4]	32.4	56.2	58.9	75.5	25.3	49.6	50.4	70.7	75.5	91.1	86.8	96.1	44.4	65.6	65.3	80.7
ScanContext [10]	86.1	89.6	88.5	91.5	91.0	91.0	92.1	92.4	96.3	97.4	96.3	97.6	91.1	92.6	92.3	93.8
Locus [12]	67.0	75.8	70.6	74.6	85.5	95.5	94.9	98.1	99.0	99.7	99.8	<b>100</b>	83.8	90.3	88.4	90.9
EgoNN [6]	98.3	<b>99.9</b>	<b>99.6</b>	99.9	95.7	97.7	96.3	98.2	97.4	98.2	97.9	98.7	97.1	98.6	97.9	98.9
LCDNet [5]	63.1	82.0	85.8	92.1	64.7	81.7	87.4	92.1	96.9	99.4	99.5	99.8	74.9	87.7	90.9	94.6
LoGG3D-Net [18]	97.7	99.7	98.8	99.8	95.2	98.4	98.2	99.2	<b>99.7</b>	<b>99.8</b>	<b>100</b>	<b>100</b>	97.5	99.3	99.0	99.6
EgoNN + SGV	<b>99.1</b>	<b>99.9</b>	<b>99.6</b>	<b>100</b>	<u>98.3</u>	<u>98.7</u>	<u>99.1</u>	<u>99.2</u>	99.2	99.4	99.7	99.7	<u>98.8</u>	<u>99.3</u>	<u>99.4</u>	<u>99.6</u>
LCDNet + SGV	90.8	92.4	94.3	95.8	90.0	90.8	95.2	95.6	<b>99.7</b>	99.7	<b>100</b>	<b>100</b>	93.5	94.3	96.5	97.1
LoGG3D-Net + SGV	<u>99.0</u>	<b>99.9</b>	99.5	<b>100</b>	<b>98.6</b>	<b>99.3</b>	<b>99.6</b>	<b>99.6</b>	<b>99.7</b>	<b>99.8</b>	<b>100</b>	<b>100</b>	<b>99.1</b>	<b>99.6</b>	<b>99.7</b>	<b>99.8</b>

TABLE II: Place recognition on the ‘easy’ evaluation set. (\*) Results are obtained from [6]. ‘R1’: Recall@1, ‘R5’: Recall@5. Bold and underline represent the best and 2nd best result respectively in each column.

	MulRan DCC					ALITA					KITTI-360				
	5 m		20 m			5 m		20 m			5 m		20 m		
	R1	MRR	$\Delta$ MRR	R1	MRR	R1	MRR	$\Delta$ MRR	R1	MRR	R1	MRR	$\Delta$ MRR	R1	MRR
ScanContext [10]	72.0	80.5	-	93.2	94.0	57.1	66.5	-	59.5	69.4	93.7	94.9	-	95.2	95.9
Locus [12]	46.3	55.6	-	71.0	77.5	95.2	97.6	-	<b>100</b>	<b>100</b>	92.7	95.1	-	97.0	98.1
EgoNN [6]	67.1	77.2	-	90.2	92.3	79.8	87.3	-	91.7	94.9	86.9	90.1	-	88.2	91.4
LCDNet [5]	57.7	71.6	-	90.9	93.8	90.5	94.6	-	96.4	97.8	85.9	89.7	-	95.7	96.6
LoGG3D-Net [18]	66.8	76.7	-	91.2	92.9	15.5	28.0	-	26.2	40.0	93.2	95.5	-	97.5	98.1
EgoNN + SGV	<u>73.6</u>	<b>82.2</b>	5.0	95.1	95.7	<b>100</b>	<b>100</b>	12.7	<b>100</b>	<b>100</b>	<u>95.7</u>	<u>96.9</u>	6.8	98.7	98.8
LCDNet + SGV	72.3	83.0	11.4	<b>99.3</b>	<b>99.4</b>	<b>100</b>	<b>100</b>	5.4	<b>100</b>	<b>100</b>	<u>95.7</u>	96.2	6.5	<u>99.0</u>	<u>99.1</u>
LoGG3D-Net + SGV	<b>73.9</b>	<u>82.0</u>	5.3	<u>96.1</u>	<u>96.5</u>	60.7	63.2	32.5	75.0	77.3	<b>96.7</b>	<b>98.1</b>	2.6	<b>99.5</b>	<b>99.5</b>

TABLE III: Place recognition on the ‘hard’ evaluation set.  $\Delta$ MRR: increase in MMR after re-ranking in 5 m threshold.

metric verification methods that do not perform registration but directly compute a spatial consistency (SC) score. Our Spectral Geometric Verification method (SpectralGV) falls into this category. We see that our method obtains significant improvements in all settings and datasets and outperforms all other re-ranking methods in Tab. IV.

All geometric verification methods show increasing re-ranking performance with increasing  $n_{topk}$ . RIR methods significantly increase computation time with increasing  $n_{topk}$  (increasing by an order of magnitude in all cases when increasing  $n_{topk}$  from 2 to 20) but our method maintains roughly constant computation time. In the  $n_{topk}=20$  setting, our method obtains the best results overall while also being more efficient than other geometric verification based methods as shown in the final row of Tab. IV operating at 3-5 ms while other GV methods take 50-300 ms. This is due to two factors, (1) our method does not need registration to perform geometric verification and (2) our method can be parallelized to process all candidates at once. The multiple registrations of RIR methods cannot be parallelized since current efficient implementations use all CPUs for a single registration.

We conduct a qualitative evaluation of re-ranking results on the 5 datasets. Fig. 3 shows point clouds corresponding to the query, initial top-1 retrieval and re-ranked top-1 retrievals in cases where an incorrect initial candidate is corrected after re-ranking. In all instances, the incorrect initial candidate point cloud is highly structurally similar to the query with only minor inconsistencies visible upon close inspection. Our re-ranking method is able to handle such complex cases and accurately identify the correct candidate.

Re-ranking enables better use of test-time knowledge.

Current retrieval methods still struggle to discriminate between complex scenes which have largely similar structural elements as they only rely on global embeddings. These ambiguities can be addressed at test time using re-ranking of the top retrieved candidates as the correct candidate is more likely to be within the top-k retrievals than top-1.

3) *Metric localization evaluation*: We compare the performance of pose estimation results for 4 methods : DH3D [4], LCDNet [5] EgoNN [6] and LoGG3D-Net [18]. All methods use RANSAC for pose estimation. Although LCDNet uses unbalanced optimal transport for transformation estimation during training, RANSAC is used during inference [5].

Table V shows 6DoF pose estimation results. We observe that in each dataset, multiple methods obtain greater than 99% success rate. This implies that given the candidate is correct (within 20 m from the query), accurately registering them is not a challenging task for state-of-the-art methods. We note that EgoNN is the most efficient method taking less than 5 ms on average. This is due to EgoNN having the lowest number of keypoints (128) and low feature dimension (128). LCDNet is the least efficient due to having the highest feature dimension (640) and using a larger number of keypoints (4096). LoGG3D-Net-sparse obtains similar success rates and run-times to EgoNN but have significantly larger RTE and RRE errors. LoGG3D-Net-dense outperforms the state-of-the-art EgoNN in all datasets, at the expense of a higher computation time. LoGG3D-Net-dense also obtains the lowest RRE and RTE errors across all datasets achieving RTE between 10-17 cm, and RRE of  $0.3^\circ$ . We attribute this to using the full resolution of the input point cloud which allows to more accurately estimate alignment (given the feature



	$n_{topk}$	MulRan DCC					ALITA					KITTI-360				
		5m		20m		t	5m		20m		t	5m		20m		t
		R1	MRR	R1	MRR		R1	MRR	R1	MRR		R1	MRR	R1	MRR	
Baseline	-	67.1	77.2	90.2	92.3	-	79.8	87.3	91.7	94.9	-	86.9	90.1	88.2	91.4	-
(a) <i>Global only:</i>																
Average-QE	2	67.4	76.7	90.2	91.8	0.2	79.8	86.5	91.7	94.3	0.1	86.9	89.3	88.2	90.8	0.2
	20	35.2	47.6	54.7	65.0	0.2	13.1	27.4	26.2	44.0	0.1	46.2	59.4	49.7	63.8	0.2
Alpha-QE [7]	2	67.4	76.7	90.6	92.0	0.2	81.0	87.1	92.9	94.9	0.1	86.7	89.2	87.9	90.6	0.2
	20	34.5	47.4	54.7	65.0	0.3	13.1	28.4	26.2	45.0	0.2	47.0	59.9	50.8	64.4	0.3
(b) <i>GV: RIR</i>																
RANSAC [21]	2	71.0	79.0	92.8	93.6	2.8	90.5	92.7	95.2	96.7	4.1	90.5	91.9	92.5	93.5	2.8
	20	<u>72.0</u>	<u>80.9</u>	<b>95.8</b>	<b>96.0</b>	63.6	<b>100</b>	<b>100</b>	<b>100</b>	<b>100</b>	60.4	<u>95.0</u>	<u>96.4</u>	<u>98.5</u>	<u>98.6</u>	56.3
FGR [36]	2	70.4	78.7	91.2	92.8	79.7	89.3	92.1	95.2	96.7	54.8	90.2	91.7	92.2	93.4	74.4
	20	70.7	78.9	92.2	93.2	175.7	97.6	98.8	<b>100</b>	<b>100</b>	126.7	93.7	95.8	98.0	98.3	171.3
TEASER++ [37]	2	70.0	78.5	92.5	93.4	26.3	90.5	92.7	95.2	96.7	30.1	89.9	91.6	92.2	93.4	35.1
	20	71.3	80.6	93.8	94.8	261.3	98.8	99.4	<b>100</b>	<b>100</b>	272.8	94.0	95.8	96.7	97.6	320.5
(c) <i>GV: SC</i>																
<b>SpectralGV (Ours)</b>	2	71.7	79.3	92.8	93.6	2.7	90.5	92.7	95.2	96.7	5.3	90.7	92.0	92.5	93.5	2.4
	20	<b>73.6</b>	<b>82.2</b>	<u>95.1</u>	<u>95.7</u>	3.0	<b>100</b>	<b>100</b>	<b>100</b>	<b>100</b>	5.7	<b>95.7</b>	<b>96.9</b>	<b>98.7</b>	<b>98.8</b>	2.8

TABLE IV: Place recognition results under different re-ranking methods using the EgoNN architecture. Methods in subsection (a) perform re-ranking using only the global descriptors. Methods in subsections (b) and (c) perform Geometric Verification (GV) based re-ranking where (b) computes the Registered-Inlier-Ratio (RIR) and (c) computes a Spatial Consistency (SC) score.  $n_{topk}$ : number of top-k retrieval candidates used during re-ranking.

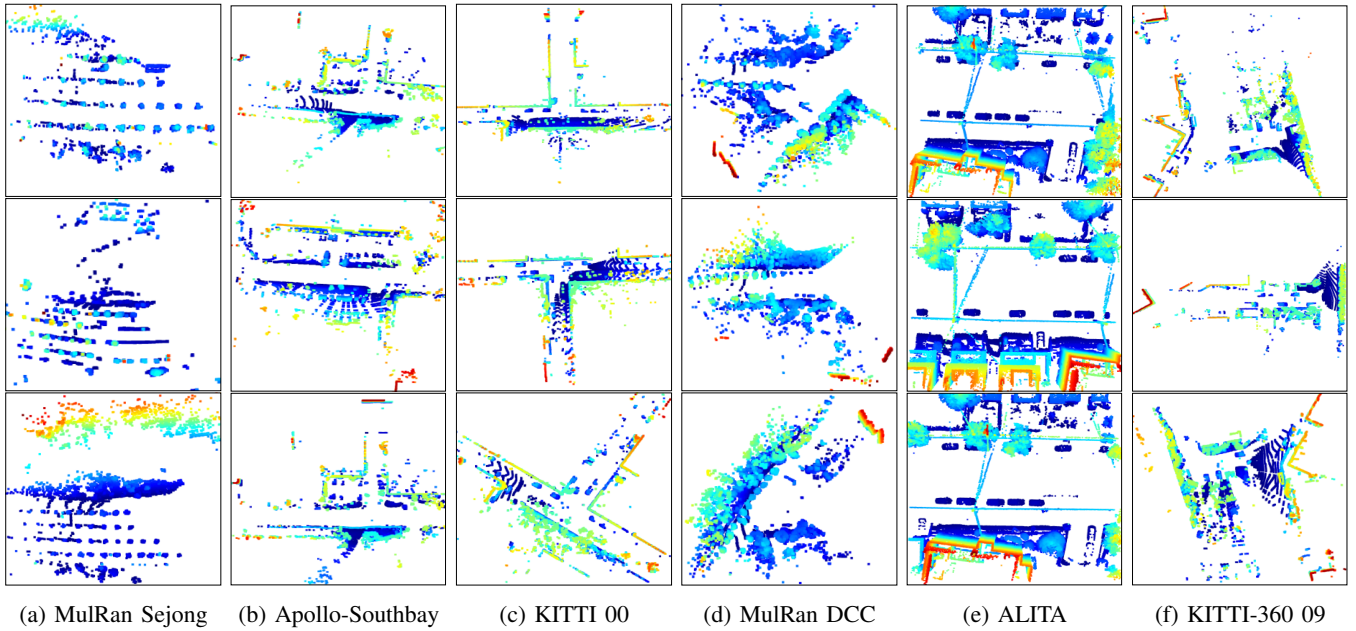


Fig. 3: Visualizations of retrieval corrections obtained using our re-ranking method on the five datasets. Top row shows the query, middle row shows the initial top1 retrieval (incorrect) and the bottom row shows the re-ranked top1 retrieval (correct). Point clouds are visualized from top-down orthogonal point of view and points are colored based on height.

	keypoint detection	num points	feature size	MulRan Sejong				Apollo-SouthBay				KITTI			
				S	RTE	RRE	t	S	RTE	RRE	t	S	RTE	RRE	t
DH3D* [4]	yes	512	128	56.3	41	1.3	-	61.4	55	0.9	-	93.2	26	0.6	-
EgoNN [6]	yes	128	128	99.6	19	0.4	<b>4</b>	99.9	<b>15</b>	0.4	<b>1</b>	99.7	<u>12</u>	<b>0.3</b>	<b>5</b>
LCDNet [5]	yes	4096	640	87.2	26	0.6	682	96.2	18	<b>0.3</b>	1,311	<b>100</b>	<u>12</u>	0.4	677
LoGG3D-Net-sparse	no	$\sim N/8$	81	99.4	50	0.6	<u>12</u>	99.0	55	0.6	20	99.8	34	0.5	9
LoGG3D-Net-dense	no	$N$	32	<b>99.8</b>	<b>17</b>	<b>0.3</b>	293	<b>100</b>	<b>15</b>	<b>0.3</b>	159	<b>100</b>	<b>10</b>	<b>0.3</b>	99

TABLE V: Results of 6DoF pose estimation under the 2m and 5° thresholds. ‘S’(↑) = Success rate (%), ‘RTE’(↓) = Relative Translation Error (cm), ‘RRE’(↓) = Relative Rotation Error(°), ‘t’(↓) = pose estimation time (ms). ‘N’ is the number of points input to the network after downsampling and ground-plane removal. (\*) Results are obtained from [6].

correspondences are sufficiently accurate).

## V. CONCLUSION

In this paper we explore re-ranking of point cloud retrievals for large-scale place recognition and metric localization. We study multiple methods for re-ranking point cloud retrieval and introduce a spectral geometric verification based re-ranking method which does not require registering the query to each candidate. Our method can be readily integrated with current metric localization methods without any changes to their architecture. We show consistent and significant performance improvements in 5 different large-scale datasets in all evaluation settings. We empirically demonstrate how, in the context of point cloud retrieval, all geometric verification methods are robust, and that our method is the most efficient method in this family. Finally, we establish new state-of-the-art results for the tasks of LiDAR-based place recognition and metric localization.

## REFERENCES

- [1] P. Yin, S. Zhao, I. Cisneros, A. Abuduweili, G. Huang, M. Milford, C. Liu, H. Choset, and S. Scherer, "General place recognition survey: Towards the real-world autonomy age," *arXiv preprint arXiv:2209.04497*, 2022.
- [2] F. Pomerleau, F. Colas, R. Siegwart *et al.*, "A review of point cloud registration algorithms for mobile robotics," *Foundations and Trends® in Robotics*, vol. 4, no. 1, pp. 1–104, 2015.
- [3] C. Park, S. Kim, P. Moghadam, J. Guo, S. Sridharan, and C. Fookes, "Robust photogeometric localization over time for map-centric loop closure," *IEEE Robotics and Automation Letters*, vol. 4, no. 2, pp. 1768–1775, 2019.
- [4] J. Du, R. Wang, and D. Cremers, "DH3D: Deep hierarchical 3d descriptors for robust large-scale 6dof relocalization," in *European Conference on Computer Vision*, 2020.
- [5] D. Cattaneo, M. Vaghi, and A. Valada, "LCDNet: Deep loop closure detection and point cloud registration for lidar slam," *IEEE Transactions on Robotics*, 2022.
- [6] J. Komorowski, M. Wysoczanska, and T. Trzcinski, "EgoNN: Ego-centric neural network for point cloud based 6dof relocalization at the city scale," *IEEE Robotics and Automation Letters*, 2022.
- [7] F. Radenović, G. Toliás, and O. Chum, "Fine-tuning cnn image retrieval with no human annotation," *IEEE transactions on pattern analysis and machine intelligence*, vol. 41, no. 7, pp. 1655–1668, 2018.
- [8] F. Tan, J. Yuan, and V. Ordonez, "Instance-level image retrieval using reranking transformers," in *Proceedings of the IEEE/CVF International Conference on Computer Vision*, 2021, pp. 12 105–12 115.
- [9] M. Leordeanu and M. Hebert, "A spectral technique for correspondence problems using pairwise constraints," in *Tenth IEEE International Conference on Computer Vision (ICCV'05) Volume 1*, 2005.
- [10] G. Kim and A. Kim, "Scan context: Egocentric spatial descriptor for place recognition within 3d point cloud map," in *2018 IEEE/RSJ International Conference on Intelligent Robots and Systems*, 2018.
- [11] G. Kim, S. Choi, and A. Kim, "Scan context++: Structural place recognition robust to rotation and lateral variations in urban environments," *IEEE Transactions on Robotics*, vol. 38, no. 3, pp. 1856–1874, 2022.
- [12] K. Vidanapathirana, P. Moghadam, B. Harwood, M. Zhao, S. Sridharan, and C. Fookes, "Locus: Lidar-based place recognition using spatiotemporal higher-order pooling," in *2021 IEEE International Conference on Robotics and Automation (ICRA)*, 2021.
- [13] M. A. Uy and G. H. Lee, "PointNetVLAD: Deep point cloud based retrieval for large-scale place recognition," in *Proceedings of the IEEE conference on computer vision and pattern recognition*, 2018.
- [14] Z. Liu, S. Zhou, C. Suo, P. Yin, W. Chen, H. Wang, H. Li, and Y.-H. Liu, "Lpd-net: 3d point cloud learning for large-scale place recognition and environment analysis," in *Proceedings of the IEEE/CVF International Conference on Computer Vision*, 2019, pp. 2831–2840.
- [15] J. Komorowski, "MinkLoc3D: Point Cloud Based Large-Scale Place Recognition," in *Proceedings of the IEEE/CVF Winter Conference on Applications of Computer Vision (WACV)*, 2021.
- [16] J. Ma, J. Zhang, J. Xu, R. Ai, W. Gu, and X. Chen, "OverlapTransformer: An Efficient and Yaw-Angle-Invariant Transformer Network for LiDAR-Based Place Recognition," *IEEE Robotics and Automation Letters*, 2022.
- [17] J. Knights, P. Moghadam, M. Ramezani, S. Sridharan, and C. Fookes, "InCloud: Incremental learning for point cloud place recognition," in *2022 IEEE/RSJ International Conference on Intelligent Robots and Systems (IROS)*, 2022.
- [18] K. Vidanapathirana, M. Ramezani, P. Moghadam, S. Sridharan, and C. Fookes, "LoGG3D-Net: Locally guided global descriptor learning for 3d place recognition," in *IEEE International Conference on Robotics and Automation (ICRA)*, 2022.
- [19] C. R. Qi, H. Su, K. Mo, and L. J. Guibas, "PointNet: Deep Learning on Point Sets for 3D Classification and Segmentation," in *IEEE Conference on Computer Vision and Pattern Recognition*, 2017.
- [20] R. Arandjelovic, P. Gronat, A. Torii, T. Pajdla, and J. Sivic, "NetVLAD: CNN architecture for weakly supervised place recognition," in *IEEE conference on computer vision and pattern recognition*, 2016.
- [21] M. A. Fischler and R. C. Bolles, "Random sample consensus: a paradigm for model fitting with applications to image analysis and automated cartography," *Communications of the ACM*, 1981.
- [22] L. Chizat, G. Peyré, B. Schmitzer, and F.-X. Vialard, "Scaling algorithms for unbalanced optimal transport problems," *Mathematics of Computation*, vol. 87, no. 314, pp. 2563–2609, 2018.
- [23] D. Qin, S. Gammeter, L. Bossard, T. Quack, and L. Van Gool, "Hello neighbor: Accurate object retrieval with k-reciprocal nearest neighbors," in *CVPR 2011*. IEEE, 2011, pp. 777–784.
- [24] Z. Zhong, L. Zheng, D. Cao, and S. Li, "Re-ranking person re-identification with k-reciprocal encoding," in *IEEE conference on computer vision and pattern recognition*, 2017.
- [25] A. Iscen, G. Toliás, Y. Avrithis, T. Furon, and O. Chum, "Efficient diffusion on region manifolds: Recovering small objects with compact cnn representations," in *Proceedings of the IEEE conference on computer vision and pattern recognition*, 2017, pp. 2077–2086.
- [26] B. Cao, A. Araujo, and J. Sim, "Unifying deep local and global features for image search," in *European Conference on Computer Vision*. Springer, 2020, pp. 726–743.
- [27] S. Hausler, S. Garg, M. Xu, M. Milford, and T. Fischer, "PatchNetVLAD: Multi-scale fusion of locally-global descriptors for place recognition," in *Proceedings of the IEEE/CVF Conference on Computer Vision and Pattern Recognition*, 2021, pp. 14 141–14 152.
- [28] S. Lee, H. Seong, S. Lee, and E. Kim, "Correlation verification for image retrieval," in *Proceedings of the IEEE/CVF Conference on Computer Vision and Pattern Recognition*, 2022, pp. 5374–5384.
- [29] X. Bai, Z. Luo, L. Zhou, H. Chen, L. Li, Z. Hu, H. Fu, and C.-L. Tai, "PointDSC: Robust point cloud registration using deep spatial consistency," in *Proceedings of the IEEE/CVF Conference on Computer Vision and Pattern Recognition*, 2021, pp. 15 859–15 869.
- [30] G. Kim, Y. S. Park, Y. Cho, J. Jeong, and A. Kim, "MulRan: Multimodal Range Dataset for Urban Place Recognition," in *2020 IEEE International Conference on Robotics and Automation*, 2020.
- [31] W. Lu, Y. Zhou, G. Wan, S. Hou, and S. Song, "L3-Net: Towards learning based lidar localization for autonomous driving," in *IEEE/CVF Conference on Computer Vision and Pattern Recognition*, 2019.
- [32] A. Geiger, P. Lenz, C. Stiller, and R. Urtasun, "Vision meets robotics: The kitti dataset," *The International Journal of Robotics Research*, vol. 32, no. 11, pp. 1231–1237, 2013.
- [33] P. Yin, S. Zhao, R. Ge, I. Cisneros, R. Fu, J. Zhang, H. Choset, and S. Scherer, "ALITA: A large-scale incremental dataset for long-term autonomy," *arXiv preprint arXiv:2205.10737*, 2022.
- [34] Y. Liao, J. Xie, and A. Geiger, "KITTI-360: A novel dataset and benchmarks for urban scene understanding in 2d and 3d," *IEEE Transactions on Pattern Analysis and Machine Intelligence*, 2022.
- [35] X. Xu, H. Yin, Z. Chen, Y. Li, Y. Wang, and R. Xiong, "Disco: Differentiable scan context with orientation," *IEEE Robotics and Automation Letters*, 2021.
- [36] Q.-Y. Zhou, J. Park, and V. Koltun, "Fast global registration," in *European conference on computer vision*, 2016.
- [37] H. Yang, J. Shi, and L. Carlone, "Teaser: Fast and certifiable point cloud registration," *IEEE Transactions on Robotics*, vol. 37, no. 2, pp. 314–333, 2020.
- [38] Q.-Y. Zhou, J. Park, and V. Koltun, "Open3d: A modern library for 3d data processing," *arXiv preprint arXiv:1801.09847*, 2018.